Semnan University

Journal of Heat and Mass Transfer Research

Journal homepage: https://jhmtr.semnan.ac.ir

ISSN: 2383-3068

Research Article

Impact of Ribs with Multiple Arrangements on the Behavior of a Turbulent Flow in a Rectangular Channel

Sarah Rabeea Nashee *, Khudheyer Salim Mushatet

Department of Mechanical Engineering, College of Engineering, University of Thi-Qar, Thi-Qar, 64001, Iraq

ARTICLE INFO

Article history:

Received: 2024-07-10

Revised: 2024-12-06

Accepted: 2025-01-04

Keywords:

Ribs turbulators;

Turbulent flow;

Thermal enhancement;

Friction factor.

ABSTRACT

This article presents a numerical analysis of the turbulent air flow in the rectangular channels equipped with ribs. The ANSYS FLUENT 17 software is used to solve the mass and momentum equations employing the finite volume approach. To get the best overall performance and to measure the pressure drop, the ribs are positioned in three different lengths. Additionally, tests and comparisons are conducted on the temperature rise of the channel wall for six alternative configurations of the ribs. The used rib lengths are 150 mm, 60 mm, and 30 mm. Experiments are conducted at the Reynolds numbers ranged from 10,000 to 35,000, pitch to rib height proportional (p/e) of 5.0, and rib height to channel height proportional (e/H) of 0.333. The results of ribs placed continuous on the upper surface of the channel and intermittent ribs placed on the lower surface of the channel in a staggered arrangement (TCBISR) case demonstrated a clear superiority when compared to the other cases evaluated, yielding the highest overall performance. Despite this instance's outstanding performance, the TCBISR case yields the highest values of friction factor.

1. Introduction

Energy efficiency is the first consideration for engineers attempting to enhance the functionality of any thermal device. It describes techniques that improve heat transfer between the fluids in heat exchangers. One of the most popular types of thermal equipment is the heat exchanger, which can be used in a wide range of sectors and applications such as power plants, air conditioning and refrigeration, food and chemicals, and automotive. A wide range of methods have been employed to enhance heat transfer in heat exchangers. One way to improve heat transmission without doing much work is to utilize rib turbulators to promote fluid mixing [1-4].

It is worth specifying that upgrading the thermal-hydrodynamic performance of the thermal systems is still an objective for numerous studies. The analysts conducted broad exploratory and explanatory studies to improve thermal performance, which affirmed that the impediments within the flow lead to an increment within the escalated turbulence of the liquid flow. For the most part, the detached strategy utilizes the insertion of balances, ribs, confuses, wires, etc. [5-7]. One of the foremost imperative passive procedures is to raise the heat transfer is employing the ribs turbulators. The foremost imperative impacts of the nearness of the ribs are to decrease the volume. Intermittent ribs are usually utilized to upgrade the heat transfer preparation in different cooling entries [8-11].

*** Corresponding author.**
E-mail address: *sara.rabee@utq.edu.iq*

Cite this article as:

Nashee, S. R. and Mushatet, K. S., 2025. Impact of Ribs with Multiple Arrangements on the Behavior of a Turbulent Flow in a Rectangular Channel. *Journal of Heat and Mass Transfer Research*, 12(2), pp. 259-270.

https://doi.org/10.22075/JHMTR.2025.34713.1575

Sahu and Bhagoria [12] examined the impact of 90° broken ribs connected to a heated absorber plate for the Reynolds number ranged from 3000 to 12000. The angle proportion of the rectangular channel had a settled value at 8 with the stature to hydraulic diameter proportion (e/Dh) of 0.0338 and harshness tallness (e) of 1.5 mm. The pitch was also ranged from 10 to 30. They concluded that there was a significant increase in Nusselt number. The maximum heat transfer coefficient was observed at a pitch of 2 cm. Furthermore, the test showed that the Nusselt number increased almost 1.25-1.4 times that of the smooth channel. Wang and Sunden [13] conducted the tests on the turbulent heat transfer in a square conduit roughened by reliable and intermittent ribs on one surface. For both cases, e/Dh of ribs was 0.15. The rib pitch proportion was 12. They observed that the heat transfer coefficient was unequivocally impacted by the shape of the ribs.

Keshmiri et al. [14] improved the heat transfer in a rectangular channel by rib-roughened surfaces for three values of pitch proportion, including p/k= 6, 9, and 12. The results showed that the pitch proportion of p/k = 9 provides the most prominent heat transfer rate. Feng et al. [15] studied the heat transfer in a system with With the internal ribs and external coolant film. They used the shear stress transport (SST) k-ω model to simulate this problem. Eren et al. [16] performed studies on the heat transfer enhancement in a rectangular channel by utilizing punctured ribs. Estimations were performed with a height proportion of 0.1 and by utilizing a joined rib pitch proportion of p/e = 12. It was found that the roughed conduit provides the heat transfer improvement of around 34.1% as compared to the smooth channel. Smaisim [17] used the rectangular channels with rectangular ribs. p/e was ranged from 6.66 to 15 in this study. It was found that the increasing the height of the ribs caused an increment in heat transfer and thermal performance of the channel. Another study was conducted by Majmader et al. [18] on a two-pass cooling channel. The effects of bidirectionally oriented ribs on the flow and heat transfer were examined in this study. h/p ratio was 10, and the channel aspect ratio was maintained at 1:2 (W: H). Three distinct cross-sectioned ribs, including square, triangular, and curved, with Reynolds numbers ranged from 10,000 to 50,000 were considered. The bi-ribbed channel has ability to create secondary flow in both horizontal as well as vertical directions. While the qualities of the square and triangle ribs are identical, the curved ribs lose 11% of their thermal performance.

Three different lengths of the ribs are arranged in different ways to reach the greatest overall performance and to investigate the pressure drop in this study. The temperature rise of the channel's wall is also compared and tested for six different arrangements of the ribs. The lengths of the ribs used are 150mm, 60mm, and 30mm. Tests are carried out at various Reynolds numbers ranged from 10000 to 35,000, pitch to the height of rib proportional of p/e=5.0, and height of rib to the height of channel proportional of e/H=0.333. These arrangements gave good improvement in the overall performance with a reasonable change in pressure drop, taking into account the advantage of ease of manufacturing and installation.

2. Mathematical Model

The geometry consists of a three-dimensional rectangular channel with the ribs turbulators arranged in parallel one by one. In this section, six cases for the ribs arrangement are considered. The first case is continuous rectangular ribs on the lower surface of the channel (CR). The second case is intermittent ribs (IR) with a particular arrangement on the lower surface. The third is intermittent and continuous ribs arranged as intermittent-continuous-intermittent (ICIR). The fourth is different intermittent ribs with two lengths (IRD). The fifth case is continuous ribs on the upper and lower surfaces in staggered arrangements (TBCSR). For the sixth case, the ribs are continuous on the upper surface of the channel and intermittent ribs are placed on the lower surface of the channel in staggered arrangements (TCBISR). The simulation has been conducted by employing Ansys Fluent. All cases are shown in Fig. 1. Figure 2 shows the details of the prameters of the study. Table 1 provides the parameters of the tested cases of rib turbulators.

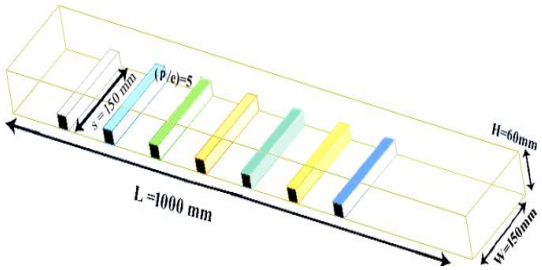

a. Continious ribs (CR)

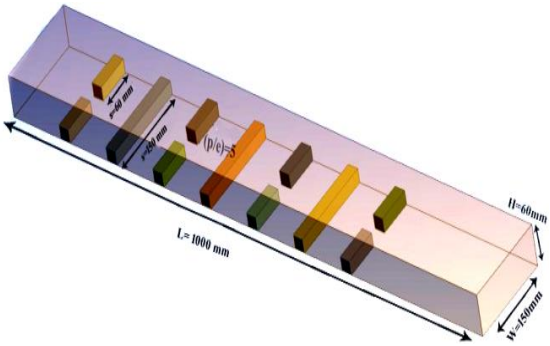

b. Continuous- intermittent-continuous ribs (ICIR)

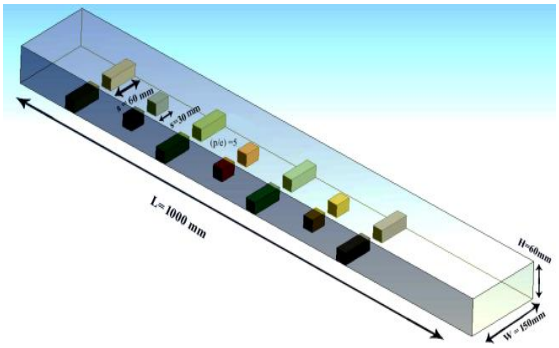

c. Intermittent ribs (IR)

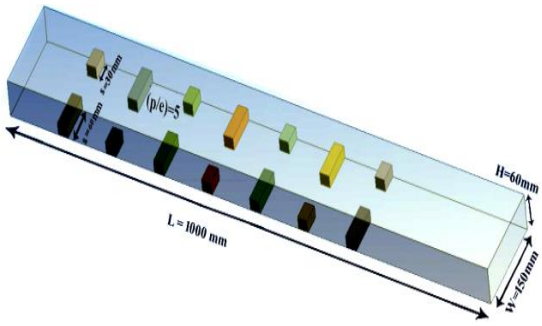

d. Intermittent ribs (IRD)

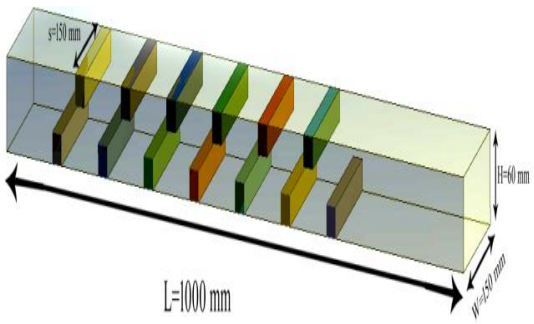

e. Continuous ribs placed on the upper and lower surfaces (TBCSR)

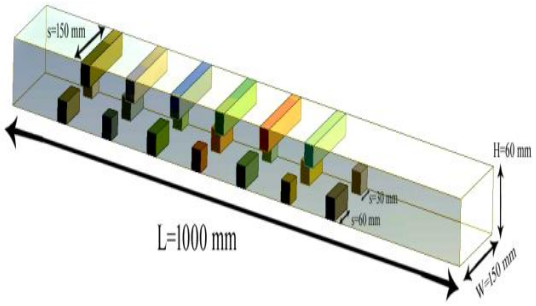

f. Continuous ribs placed on the upper surface and intermittent ribs placed on the lower surface (TCBISR)

Fig. 1 The schematic diagram of test cases

Table 1. Geometrical parameters for the physical model

The tested channel			
Length (L)			1000 mm
Height (H)			60 mm
Width (W)			150 mm
Thickness			2 mm
The cases of arrangement			
Cases	**e/H**	**p/e**	**s (length of ribs)**
(CR)	0.33	5	150 mm
(ICIR)			150 mm and 60 mm
(IRD)			60 mm and 30 mm
(IR)			30 mm
(TBCSR)			150 mm
(TCBISR)			150 mm, 60 mm and 30 mm

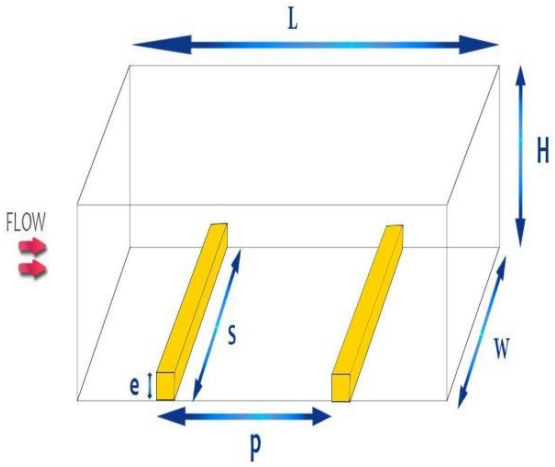

Fig. 2. The details of parameters

2.1. Governing Equations

The continuity, momentum, and energy equations can be used in depicting the turbulent flows and heat transfer. In this study, they used to discuss the turbulence flow and heat transfer in the three-dimensional rectangular channel with the ribs turbulator.

The continuity equation is a mathematical expression representing the conservation of mass [19].

$$\frac{\partial u}{\partial x}+\frac{\partial v}{\partial y}+\frac{\partial w}{\partial z}=0 \tag{1}$$

The Navier-Stokes equations (N-S) are [20]:

In *x*-direction:

$$\rho\left(\frac{\partial u^2}{\partial x}+\frac{\partial uv}{\partial y}+\frac{\partial uw}{\partial z}\right)=-\frac{\partial P}{\partial x}+\frac{\partial}{\partial x}\left(\mu_{eff}\frac{\partial u}{\partial x}\right)+\frac{\partial}{\partial y}\left(\mu_{eff}\frac{\partial u}{\partial y}\right)+\frac{\partial}{\partial z}\left(\mu_{eff}\frac{\partial u}{\partial z}\right) \tag{2}$$

In *y*-direction:

$$\rho\left(\frac{\partial vu}{\partial x}+\frac{\partial v^2}{\partial y}+\frac{\partial vw}{\partial z}\right)=-\frac{\partial P}{\partial y}+\frac{\partial}{\partial x}\left(\mu_{eff}\frac{\partial v}{\partial x}\right)+\frac{\partial}{\partial y}\left(2\mu_{eff}\frac{\partial v}{\partial y}\right)+\frac{\partial}{\partial z}\left(\mu_{eff}\frac{\partial v}{\partial z}\right) \tag{3}$$

In *z*-direction:

$$\rho\left(\frac{\partial wu}{\partial x}+\frac{\partial wv}{\partial y}+\frac{\partial w^2}{\partial z}\right)=-\frac{\partial P}{\partial z}+\frac{\partial}{\partial x}\left(\mu_{eff}\frac{\partial w}{\partial x}\right)+\frac{\partial}{\partial y}\left(\mu_{eff}\frac{\partial w}{\partial y}\right)+\frac{\partial}{\partial z}\left(\mu_{eff}\frac{\partial w}{\partial z}\right) \tag{4}$$

The energy equation is the mathematical relation that represents energy conservation [21].

$$\frac{\partial uT}{\partial x}+\frac{\partial vT}{\partial y}+\frac{\partial wT}{\partial z}=\frac{\partial}{\partial x}\left(\Gamma_{eff}\frac{\partial T}{\partial x}\right)+\frac{\partial}{\partial y}\left(\Gamma_{eff}\frac{\partial T}{\partial y}\right)+\frac{\partial}{\partial z}\left(\Gamma_{eff}\frac{\partial T}{\partial z}\right) \tag{5}$$

The standard model is valid only for turbulent flows. For turbulent kinetic energy (k) [22]:

$$\rho\left(\frac{\partial}{\partial x}(ku)+\frac{\partial}{\partial y}(kv)+\frac{\partial}{\partial z}(kw)\right)=\frac{\partial}{\partial x}\left(\frac{\mu_t}{\sigma_k}\frac{\partial k}{\partial x}\right)+\frac{\partial}{\partial y}\left(\frac{\mu_t}{\sigma_k}\frac{\partial k}{\partial y}\right)+\frac{\partial}{\partial z}\left(\frac{\mu_t}{\sigma_k}\frac{\partial k}{\partial z}\right)+G-\rho\varepsilon \tag{6}$$

For energy dissipation rate (ε) [23]:

$$\rho\left(\frac{\partial}{\partial x}(\varepsilon u)+\frac{\partial}{\partial y}(\varepsilon v)+\frac{\partial}{\partial z}(\varepsilon w)\right)=\frac{\partial}{\partial x}\left(\frac{\mu_t}{\sigma_\varepsilon}\frac{\partial \varepsilon}{\partial x}\right)+\frac{\partial}{\partial y}\left(\frac{\mu_t}{\sigma_\varepsilon}\frac{\partial \varepsilon}{\partial y}\right)+\frac{\partial}{\partial z}\left(\frac{\mu_t}{\sigma_\varepsilon}\frac{\partial \varepsilon}{\partial z}\right)+\rho\frac{\varepsilon}{k}G-C_{1\varepsilon}\rho\frac{\varepsilon}{k} \tag{7}$$

where G is the generation term defined by [23]:

$$G=\mu_t\left[2\left(\frac{\partial u}{\partial x}\right)^2+2\left(\frac{\partial v}{\partial y}\right)^2+2\left(\frac{\partial w}{\partial z}\right)^2+\left(\frac{\partial v}{\partial y}+\frac{\partial u}{\partial x}\right)^2+\left(\frac{\partial v}{\partial z}+\frac{\partial w}{\partial x}\right)^2+\left(\frac{\partial v}{\partial z}+\frac{\partial w}{\partial y}\right)^2\right] \tag{8}$$

The heat transfer coefficient can be calculated by [25]:

$$\bar{h}=\frac{q}{T_w-T_b} \tag{9}$$

The overall bulk temperature of the fluid is calculated in Fluent by volume integral and mass-weighted average, as follows [26]:

$$T_b=\frac{\int_0^L\int_0^H\int_0^W \rho\ c_p\ uT\ dx\ dy\ dz}{\int_0^L\int_0^H\int_0^W \rho\ u\ dx\ dy\ dz} \tag{10}$$

The average wall temperature is calculated by surface integral and area-weighted average, as follows [27]:

$$T_w=\frac{1}{A}\int T_i dA_i=\frac{1}{A}\sum_{i=1}^{n} T_i|A_i| \tag{11}$$

The friction factor is defined by using the Darcy Weisbach equation [28]:

$$f=\frac{\Delta P\ .D_h}{\frac{1}{2}\rho\ u_{avg}^2\ .\ L} \tag{12}$$

P_{in} was calculated by surface integral and area-weighted average, as follows [29]:

$$P=\frac{1}{A}\int P_i\ dA_i=\frac{1}{A}\ \sum_{i=1}^{n} P_i\ |A_i| \tag{13}$$

P_{out} was specified as a boundary condition and was selected as zero Pascal.

The mean Nusselt number (Nu) [30] is estimated as follows:

$$Nu=\frac{\bar{h}\ .D_h}{k} \tag{14}$$

Overall performance is considered here as a measure of improving the overall performance of the channel [31]:

$$\eta=(Nu_w/Nu_0)\ /\ (f_w/f_0)^{1/3} \tag{15}$$

2.2. Mesh Generation

Discretization in space requires that the flow field ought to be separated into little control volumes. Diverse sorts of control volumes are conceivable, including hexahedral and tetrahedral control volumes and organized or unstructured networks. The tetrahedral mesh is utilized in this study, as appeared in Fig. 3, since it is good for the separated flow simulation. It is evident that the mesh should be fine enough for the regions near the dividers and the ribs

turbulator to capture the flow action in these areas. Nu and *f* were used to perform the grid independence test at Re = 20000. The number of grids was raised in the grid independence test until there was little change in the results between two successive grid sizes. Table 2 provides a summary of the findings of the grids for each form and arrangement.

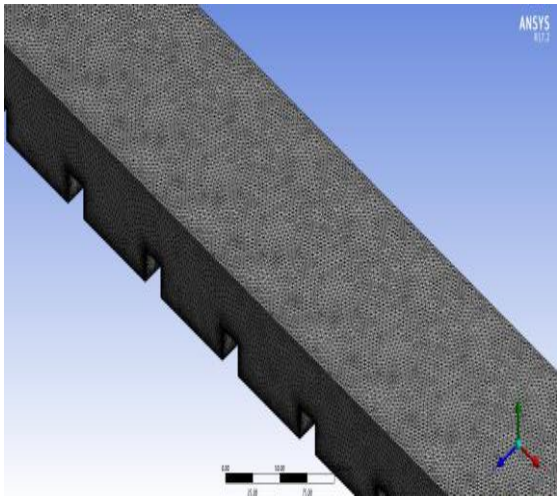

Fig. 3. The mesh generated in the computational domain

Table 2. Different grids and their Nu and fr for different cases at Re= 20,000.

Case	Number of grid elements	Nu	f
Smooth channel	592,222	57.6001	0.032
	631,180	58.7313	0.0332
	724,800	59.0212	0.0336
	824,822	59.1065	0.034
CR [p/e=5, e/H=0.33, and s= 150 mm]	2,210,733	92.0123	0.0563
	2,344,658	90,684	0.0571
	2,412,236	89.559	0.0576
	2,549,349	88,782	0.058
ICIR [p/e=5, e/H=0.33, and s= 150, 60 mm]	2,465,253	91.66	0.068
	2,486,390	92.78	0.071
	2,524,667	93.34	0.074
	2,579,547	93.82	0.075
IR [p/e=5, e/H=0.33, and s= 60, 30 mm]	2,524,244	90.83	0.056
	2,553,988	91.877	0.059
	2,627,675	92.331	0.062
	2,679,453	92.66	0.063
IRD [p/e=5, e/H=0.33, and s= 60, 30 mm]	2,577,377	100.832	0.08
	2,627,738	103.204	0.083
	2,747,589	101.98	0.081
	2,810,848	102.88	0.082
TBCSR [p/e=5, e/H=0.33, and s= 150 mm]	3,423,840	118.482	0.087
	3,492,000	120.765	0.095
	3,624,220	122.453	0.101
	3,755,559	123.551	0.104
TCBISR [p/e=5, e/H=0.33, and s= 150, 60, 30mm]	3,930,800	127.175	0.1411
	4,017,764	129.821	0.152
	4,288,011	128.726	0.1446
	4,583,353	129.122	0.151

2.3. Boundary Conditions

The following boundary conditions are used in this study:

1) Uniform inlet velocity, u = u_{in} (1.751 m/sec to 6.12 m/sec).
2) Walls, noo slip boundary condition, u=v=w=0.
3) A smooth exit for the dependent variable ($\frac{\partial u}{\partial x} = \frac{\partial v}{\partial y} = \frac{\partial w}{\partial z} = 0$) is assumed.
4) Inlet temperature (T_{in}=300K).
5) A zero gauge pressure is specified at the outlet domain.
6) Constant heat flux =1000W/m^2 on walls.

3. Results and Discussion

Every arrangement is compared separately against both the continuous ribs case and the smooth channel case. When testing p/e and e/H proportions, the case with persistent ribs was selected because it demonstrated the highest overall performance. The best channel execution within the proximity of continuous ribs was at p/e=5.0 and e/H=0.333. This particular scenario has been selected as a basis for comparison with the alternative strategies.

For investigating the effect of ICIR case on wall temperature, figure 4 displays the results reported for the mean wall temperature. It can be seen that the wall temperature reduces with increasing Reynolds number. There are differences between the wall temperature values for different cases. The decrease in the wall temperature values for the case of ICIR is 8% compared to the case of CR case and 28% compared to the smooth channel.

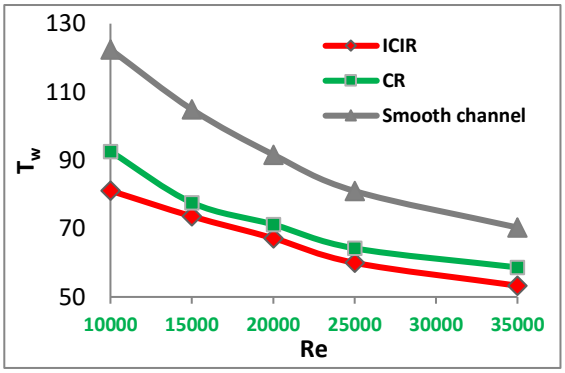

Fig. 4. The variation of T_w with Reynolds numbers for cases of ICIR, CR, and smooth channel

This decrease in the mean wall temperature of ICIR case as compared to the smooth channel and CR cases is due to an increase in the mixing and recirculation, which results in better heat transfer. The mixing caused by these ribs

reduces the temperature of the heated surface due to the heat transfer that occurs between the surface and the fluid flow. The findings additionally demonstrated that, in comparison to the smooth channel case and the CR case, the ICIR case has larger friction factor (f) for all values of Reynolds number considered. This is due to the obstruction provided by the ribs against the fluid flow, which raises surface resistance and represses the viscous sublayer. This causes a drop in pressure, which raises the values of the friction factor. When comparing with the CR and the smooth channel cases, the increase in the friction factor values for the ICIR case is 29% and 55%, respectively. The differences between the cases are shown in Fig. 5.

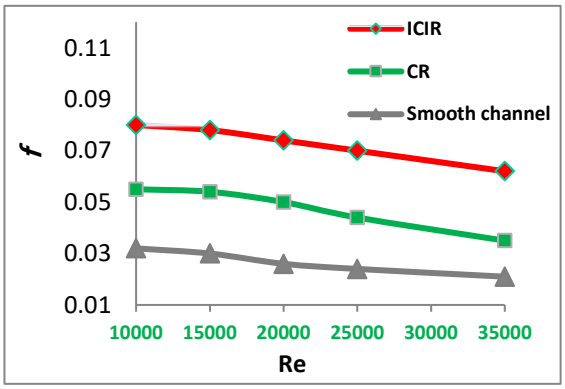

Fig. 5. The variation of friction factor with Reynolds numbers for cases of ICIR, CR, and smooth channel

As for the comparison of the values of friction factor for IR case, the values varied for all cases, where IR case has the maximum values of friction factor. The increase of friction factor for the IR case is 20% as compared with CR case and is 52 % as compared with the smooth channel case. Figure 6 describes the difference between the results of three cases for the friction factor. The increase of friction factor for the IR case compared to CR and smooth channel cases may be due to the exist of the intermittent-ribs, which seperates the fluid flow. This results in creation of a larger recirculation zone behind the rib.

For the mean wall temperature, figure 7 displays the effect of the IR case on the wall temperature for different Reynolds numbers. The results are compared with CR and smooth channel cases in this figure. It can be observed that the mean wall temperature decreases with increasing the Reynolds number. Moreover, IR case shows less growth in wall temperature as compared with the other cases. The decrease in the wall temperature values for IR case is 6.5% as compared with CR case and IS 26% as compared with the smooth channel case. This is due to the fact that the IR case provides greater mixing due to greater air obstruction. This leads to better heat transfer between the surface and air flow.

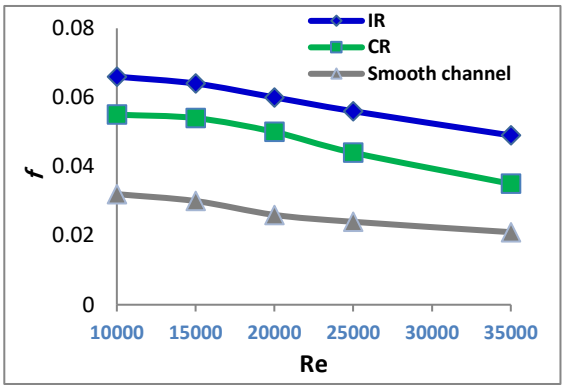

Fig. 6. The variation of friction factor with Reynolds numbers for cases of IR, CR, and smooth channel

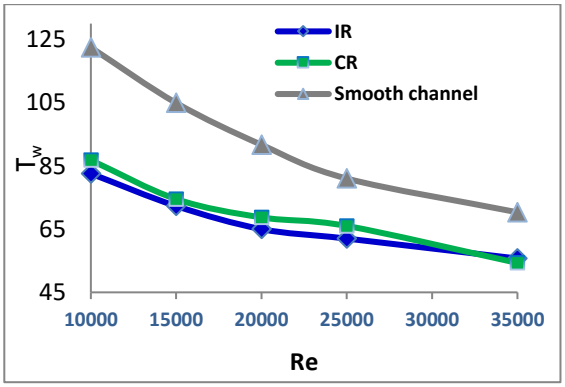

Fig. 7. The variation of T_w with Reynolds numbers for cases of IR, CR, and smooth channel

The effects of IRD case on the friction factor are shown in Fig. 8. It is obvious that friction factor reduces with increasing the Reynolds number. In addition, by comparing the results of IRD, CR, and smooth channel cases, it is found that the IRD case has a greater friction factor than two other cases. The increase in friction factor for IRD case is 32 % compared with CR case and is 62% compared to smooth channel case. The increment in friction factor for IRD case compared to CR and smooth channel cases is due to the presence of the intermittent ribs. Such ribs causes high turbulence and can initiate a bigger recirculation zone behind the rib driving to higher vortex quality and this leads to increase the pressure drop.

As for mean wall temperature, the variation of T_w with the Reynolds number for IRD, CR, and smooth channel cases are shown in Fig. 9. T_w reduces as the Reynolds number increases. It is noticed that T_w for the case of IRD is 9% and 31% smaller than that of for the CR and the smooth channel cases, respectively. This is due to the increasing in heat transfer between the hot surface and the air flow in IRD case that leads to a decrease in mean wall temperature.

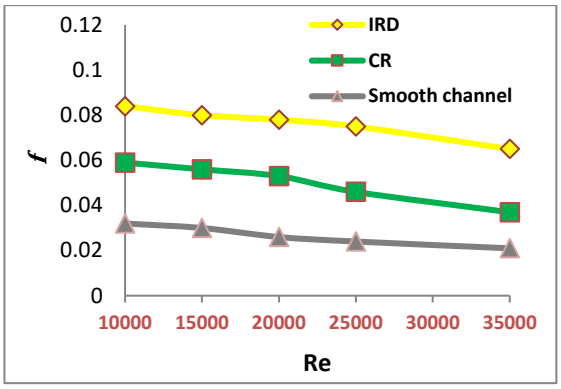

Fig. 8. The variation of friction factor with Reynolds numbers for cases of IRD, CR, and smooth channel

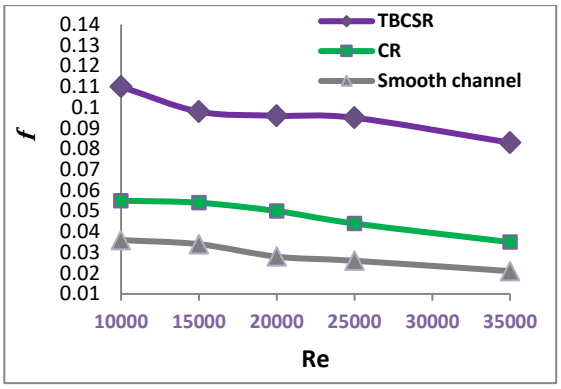

Fig. 10. The variation of friction factor with Reynolds numbers for cases of TBCSR, CR, and smooth channel

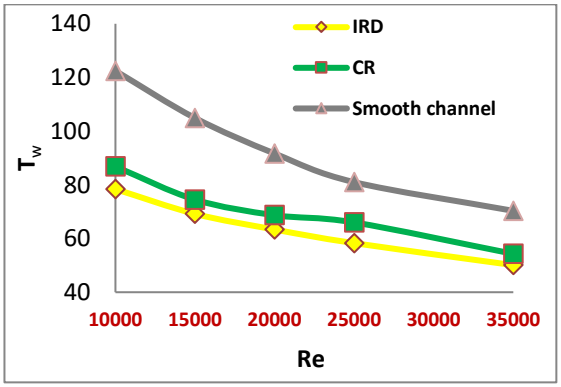

Fig. 9. The variation of T_w with Reynolds numbers for cases of IRD, CR, and smooth channel

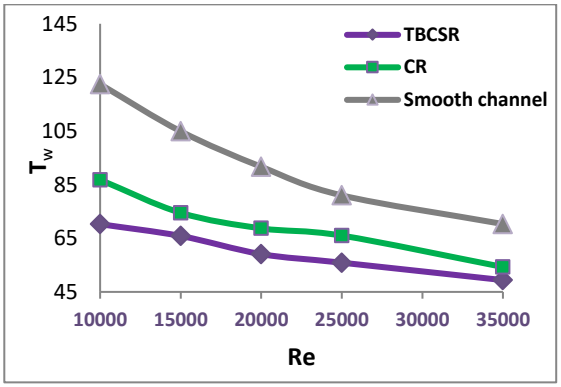

Fig. 11. The variation of T_w with Reynolds numbers for cases of TBCSR, CR, and smooth channel

Figure 10 shows the effects of the arrangement of TBCSR case on the friction factor for various values of Reynolds number. Results of friction factor obtained for TBCSR case are compared with CR and smooth channel cases. It is found that the friction factor for TBCSR case is greater about 50% and 69% than those for CR and smooth channel cases, respectively. This is due to the fact that the high turbulence can induce a greater recirculation zone behind the rib, leading to greater strength of vortices, and this causes a rise in the pressure drop.

In regard to T_w, Fig. 11 displays the effect of the arrangement of TBCSR case on the T_w for different Reynolds number with a comparison with CR and smooth channel cases. The results show that T_w reduces with increasing the Reynolds number. Furthermore, TBCSR case indicates less growth in T_w as compared with other cases. The decrease in T_w for TBCSR case is 13.7% compared to CR case and 35.7% compared with the smooth channel case. The obstruction on the two of the channel's surfaces results in more heat transfer, which enhances the heat transfer between the heated surfaces.

The effect of the arrangement of TCBISR case on friction factor for various values of Reynolds number is shown in Fig. 12. It is obvious that friction factor reduces with increasing the Reynolds number. In addition, by comparing the results of TCBISR, CR, and smooth channel cases, it is found that the arrangement of TCBISR produces a greater friction factor than two other cases. The outcomes show that the friction factor values for TCBISR case is 54% higher as compared with CR case and 72% higher ascompared with the smooth channel case. As the friction factor represents the pressure drop (Δp) in the channel, the rise in friction factor values for TCBISR case can be attributed to the same fact. The high turbulence results in a larger recirculation zone behind the rib, leading to greater vortex strength, and this leads to a rise in the pressure drop.

For the mean wall temperature, Fig. 13 shows the impact of the TCBISR case on T_w for different Reynolds number with a comparison with CR and smooth channel cases. The results show that T_w diminishes with increasing the Reynolds number.

Besides, TCBISR case shows less development in mean wall temperature as compared with other cases. The obtained results indicate that the decrease of the wall temperature values for TCBISR case is 19% as compared with CR case and is 39% as compared with the smooth channel case. The decrease in the wall temperature of TCBISR case is due to a strong mixing fluid, which leads to quicker extrication from the hot surface. Due to the additional impact of these ribs on the heat transfer and the preference for employing the discontinuous ribs at the bottom over the prior case, the figure illustrates the difference in values. In this instance, there was a noticeable variation in heat transfer.

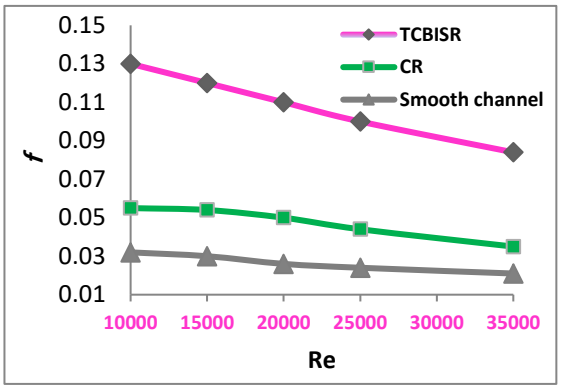

Fig. 12. The variation of friction factor with Reynolds numbers for cases of TCBISR, CR, and smooth channel

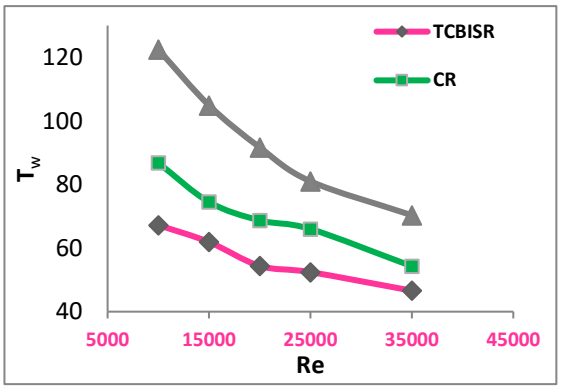

Fig. 13. The variation of T_w with Reynolds numbers for cases of TCBISR, CR, and smooth channel

When comparing the results of all cases tested, the superiority was clear for the outcomes of the TCBISR case, as it gives the highest overall performance at a Reynolds number of 10,000, reaching 1.8 %. As Fig. 14 shows, the thermal performance is in the form of a downward slope and declines with increasing the Reynolds number.

Figure 15 displays the effects of different arrangement of the ribs on Nu/ΔP ratio for different values of Reynolds number. The results indicate that TCBISR case has the smallest values of Nu/ΔP for all values of Reynolds number. The ratio ranged from 16.6 to 2.5 as the Reynolds number increases from 10,000 to 3,5000. At the same time, CR case has the highest values of Nu/ΔP for all values of Reynolds number. The ratio ranged from 27 to 9.6 as the Reynolds number is increased from 10000 to 35000. This difference is due to the variation of Nusselt number and the difference in the heat transfer rate of each case, where TCBISR case gives the highest heat transfer while CR case gives the lowest heat transfer rate. In addition, it is due to the difference in the pressure drop, where the pressure drop increases with an rise in the heat transfer for every case and also with the velocity of the air.

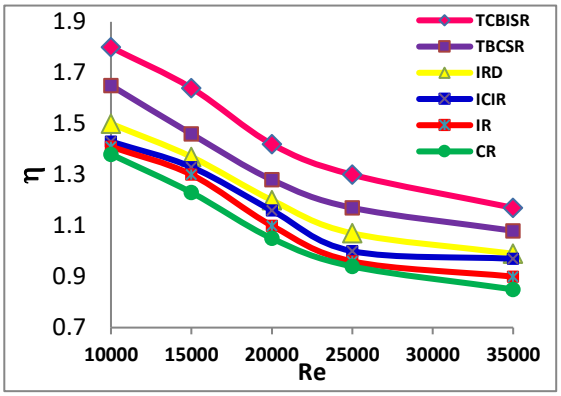

Fig. 14. The variation of the thermal performance with Reynolds number for different arrangements of ribs

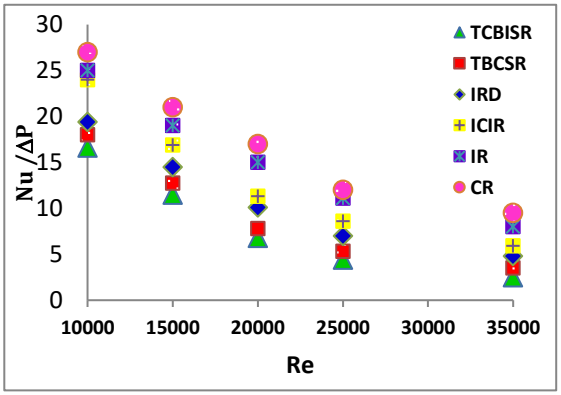

Fig. 15. The variation of Nu/ΔP with Reynolds number for different arrangements of ribs

Figure 16 shows the relationship between (T_w-T_b) and Reynolds number for all arrangements considered. The results indicate a valuable decrease in the values of (T_w-T_b) for TCBISR case, where it is ranged from 35.03 to 20.3 as Reynolds number increases from 10000 to 35000. The CR case gives the smallest values of (T_w-T_b), ranged from 57.41 to 33.3 as the Reynolds number increases from 10000 to 35000. By decreasing the value of (T_w-T_b), there is uniformity in temperature, and the rate of heat transfer increases, so that TCBISR gives the highest heat transfer as compared to the other cases.

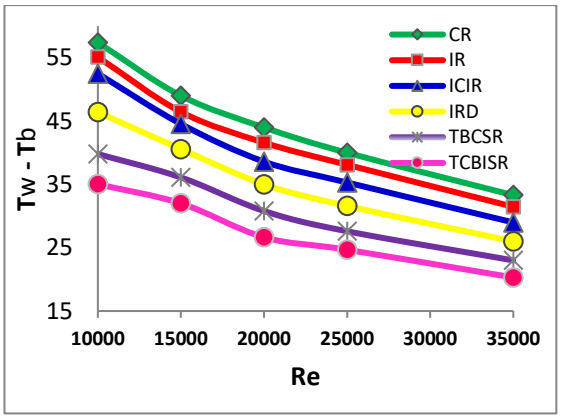

Fig. 16. The variation of ($T_w - T_b$) with Reynolds number for different arrangements of ribs

3.1. Reduction in length

To investigate the reduction of the channel length (1 m), a specific value of heat transfer rate (Q=140W) at Re= 10,000 has been selected for several cases considred in this study. The reduction in length for all studied cases is shown in Fig. 17. For the exact amount of heat transfer for all studied cases, the reduction in length is about 15%, 21%, 19%, 26%, 36%, and 42% for CR, ICIR, IR, IRD, TBCSR, and TCBISR cases, respectively. The results indicate that the heat transfer rate of Q=140 W can be obtained with 85 cm, 79 cm,82 cm, 74 cm, 64 cm, and 58 cm lengths of the channel for CR, ICIR, IR, IRD, TBCSR, and TCBISR cases, respectively. As a result, the TCBISR case has the maximum reduction in the size of the channel as compared with the other cases, while CR has the lowest reduction in the size of the channel.

The reduction in length (L.R) of the channel is calculated by:

$$L.R = (L-L_x)/L$$

where L is the total length of the channel and L_x is the required length of the channel to give the same amount of heat transfer as the total length.

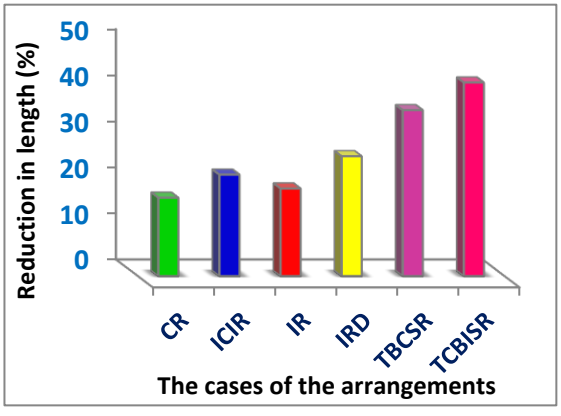

Fig. 17. The reduction in length for different arrangements of ribs

Figures 18, 19, and 20 show a comparison between the results of this study and the published results of Gupta et al. [32]. The validations have been conducted for the Nusselt number, friction factor, and η. The tests conducted for a channel with transverse ribs arranged with p/e = 10 and e/Dh = 0.06, both with and without a gap. The case with 90o angle of attack was selected. It can be seen that the results have only the slight differences of 15%, 16%, and 7% for the Nusselt number, friction factor, and η, respectively. Different pitch ratio values and channel layouts can be the sources of this discrepancy.

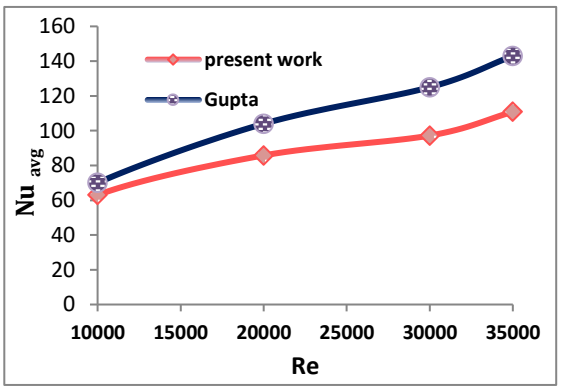

Fig. 18. Comparison between the results of current study and Gupta et al. [32] for Nusselt number

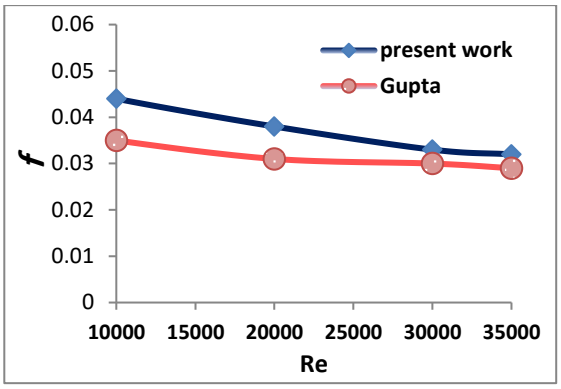

Fig. 19. Comparison between the results of current study and Gupta et al. [32] for friction factor

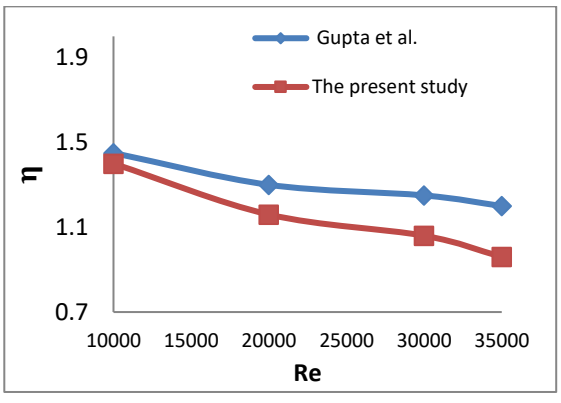

Fig. 20. Comparison between the results of current study and Gupta et al. [32] for η

4. Conclusions

From the outcomes of the current simulation, the following results are acheived:

1) In general, the outcomes indicate that the Nusselt number is better in the case of TCBISR. This is due to the raised in the mixing of the air, which provided a greater opportunity for heat transfer due to the formation of larger vortices and a rising in the recirculation area. The maximum Nusselt number for the case of TCBISR was observed at Re=35,000.
2) The maximum overall performance of the channel obtained is 1.8% for the case of TCBISR at Re=10,000.
3) The maximum friction factor value obtained is 0.12 for the case of TCBISR at Re=10,000. Therefore, it must be noted that the increase in the overall performance of the channel was accompanied by a rise in pressure drop (Δp) and friction factor (f).
4) The lowest friction factor and overall performance is observed in the case of CR.
5) TCBISR has the maximum reduction in size of channel as compared with the other cases, while CR has the lowest reduction in size of channel. As a result, this case can save cost and size.

5. Recomendations

Holes can be added to the ribs to increase the turbulence and thus improve heat transfer. The ribs used can also be arranged with different angles in future studies.

Nomenclatur

A	Cross section area [m^2]
D_h	Hydraulic diameter, m
e	Rib height, m
f	Friction factor
h	Convective heat transfer coefficient,
H	Channel height, m
K	Thermal conductivity, W/mK
L	Length of channel, m
Nu	Nusselt number
p	Pitch of ribs, m
P	Pressure, Pa
Re	Reynolds number
T	Temperature, K
η	Overall performance

Funding Statement

This research did not receive any specific grant from funding agencies in the public, commercial, or not-for-profit sectors.

Conflicts of Interest

The author declares that there is no conflict of interest regarding the publication of this article.

Authors Contribution Statement

Sarah Rabeea Nashee: Conceptualization; Data Curation; Formal Analysis; Investigation; Methodology; Project Administration; Resources; Software.

Khudheyer Salim Mushatet: Supervision; Validation; Visualization; Writing, Review & Editing.

References

[1] Kamal Fahad, M., Farhan Ifraj, N., Huda Tahsin, S., Jahid Hasan, Md., 2023. Numerical investigation of the hydrothermal performance of novel vortex generators in a rectangular channel by employing inclination and rotational angles. International Journal of Thermofluids, 20, 100500.

[2] Deshmukh, P.W., and Lahane, S., 2024. Numerical evaluation of novel curved rib turbulators for thermal performance improvement in circular geometries. Heat Transfer Engineering, 45(6), pp. 528-551.

[3] Mushatet, K.S., and Hmood, H.M., 2021. Numerical investigation for heat transfer enhancement in a triangular twisted tube. ARPN Journal of Engineering and Applied Sciences, 16(5) pp. 593-599.

[4] Mansour, M.M., Hamood, H.M., Lafta, A.M., Nashee, S.R., 2024. Enhancing the efficacy of adsorption-based carbon storage systems: a finite element analysis approach. International Journal of Energy Production and Management, 9(1), pp. 19-24.

[5] Rahman, Md.A. and Dhiman, S.K., 2024. Thermo-fluid performance of a heat exchanger with a novel perforated flow deflector type conical baffles. Journal of Thermal Engineering, 10(4), pp. 868-879.

[6] Mushatet, K.S., and Nashee, S., 2021. Experimental and computational investigation for 3-D duct flow with modified arrangement ribs turbulators. Thermal Science, 25(3), pp. 1653-1663.

[7] Oztop, H.F., Mushatet, K.S., Yılmaz, I., 2012. Analysis of turbulent flow and heat transfer over a double forward facing step with obstacles. International Communications in Heat and Mass Transfer, 39(9), pp. 1395-1403.

[8] Mushatet, K.S. 2011. Simulation of turbulent flow and heat transfer over a backward facing step with ribs turbulators. Thermal Science, 15(1), pp. 245-255.

[9] Nashee, S.R., 2024. Numerical simulation of heat transfer enhancement of a heat exchanger tube fitted with single and double-cut twisted tapes. International Journal of Heat and Technology, 42(3), pp. 1003-1010.

[10] Mansour, M.M., Salman, H.S., Lafta, A.M., Nashee, S.R., Shkarah, A.J., 2024. Simulation analysis of protection oil pipe in platform to reduced corrosion and erosion defect with sustainability technique. Mathematical Modelling of Engineering Problems, 11(5), pp. 1171-1178 .

[11] Majmader, F.B., and Hasan, Md.J., 2024. Multi-objective hydrothermal performance optimization of a microchannel heat sink equipped with delta winglet vortex generators using NSGA-II genetic algorithm. International Journal of Thermal Sciences, 201, 109046.

[12] Sahu, M.M. and Bhagoria, J.L., 2005. Augmentation of heat transfer coefficient by using 90 broken transverse ribs on absorber plate of solar air heater. Renewable Energy, 30(13), pp. 2057-2073.

[13] Wang, L., and Sunden, B., 2007. Experimental investigation of local heat transfer in a square duct with various-shaped ribs. Heat and Mass Transfer, 43(8), pp. 759-766.

[14] Keshmiri, A., Cotton M.A., Addad, Y., 2009. Numerical simulations of flow and heat transfer over rib-roughened surfaces. Paper CFDSC2009-3D3, Proc. 17th Ann. Conf. of the CFD Society of Canada, Ottawa, Canada.

[15] Feng, Z., Dou, Z., Wang, J., Ma, S., Zhang, Z., 2012. Numerical investigation of cooling enhancement with internal ribs coolant film. In Proceedings, ASME Turbo Expo, Copenhagen, Denmark.

[16] Eren, S., Caliskan S., Zirzakiran M., 2015. Experimental investigation of heat transfer in a rectangular channel with perforated ribs. The Online Journal of Science and Technology *(Tojsat*), 5(3), pp. 37-44.

[17] Smaisim, G.F., 2018. Investigation on heat transfer augmentation using continuous and broken ribs on a plate of heat exchanger. International Journal of Energy & Environment, 9(3), pp. 211-232.

[18] Majmader, F.B., and Hasan, Md.J., 2024. Effects of bidirectional rib arrangements on turbulent flow structure and heat transfer characteristics of a two-pass channel for turbine blade internal cooling. International Communications in Heat and Mass Transfer, 156, 107688.

[19] Nashee, S.R., 2024. Enhancement of heat transfer in nanofluid flow through elbows with varied cross-sections: A computational study. International Journal of Heat and Technology, 42(1), pp. 311-319.

[20] Hamood, H.M., Mansour, M.M., Lafta, A.M., Nashee, S.R., 2024. Numerical investigation to study the effect of three height of triangular obstacles on heat transfer of nanofluids in a microchannel. International Review of Mechanical Engineering (IREME). 17(11).

[21] Nashee, S.R., 2023. Numerical study for fluid flow and heat transfer characteristics in a corrugating channel. International Journal of Heat & Technology ,41(2), p.392.

[22] Mushatet, K.S., 2011. Simulation of turbulent flow and heat transfer over a backward facing step with ribs turbulators. Thermal Science, 15(1), pp. 245-255.

[23] Nashee, S.R., and Hmood, H.M., 2023. Numerical study of heat transfer and fluid flow over circular cylinders in 2D cross flow. Journal of Advanced Research in Applied Sciences and Engineering Technology, 30(2), pp. 216-224.

[24] Nashee, S., and Mushatet, K.S., 2024. Performance study on turbulent heat transfer using rectangular air duct integrated with continuous and intermittent ribs turbulators. Thermal Science, doi: 10.2298/TSCI240430214N.

[25] Hossain, J., Curbelo, A., Garrett, C., Wang, W., Kapat, J., Thorpe, S., Maurer, M., 2017. Use of rib turbulators to enhance postimpingement heat transfer for curved surface. Journal of Engineering for Gas Turbines and Power, 139(7), 071901.

[26] Abdul Razzaq, A.K., and Mushatet, K.S., 2023. Influence of the twisting and nano fluids on performance of a triangular double tube heat exchanger. Kerntechnik, doi: https://doi.org/10.1515/kern-2023-0132.

[27] Nashee, S.R., Ibrahim, Z.A., Kamil, D.J., 2024. Numerical investigation of flow in vertical rectangular channals equipped with three different obstacles shape. AIP conference proceeding Fourth International Conference On Advances In Physical Sciences And Materials: Icapsm 2023, 17–18 August 2023, Coimbatore, India, Volume 3122, Issue 1.

[28] Venkatesh, G., Meenakshi Reddy, R., Rao, P.M., 2024. Improving thermal performance of turbine blade with combination of circular and oblong fins in a wedge channel: a numerical investigation. International Journal of Turbo & Jet-Engines, 2024, doi: ttps://doi.org/10.1515/tjj-2024-0010.

[29] Abraham, S., and Vedula, R.P., 2016. Heat transfer and pressure drop measurements in a square cross-section converging channel with V and W rib turbulators. Experimental Thermal and Fluid Science, 70, pp. 208-219.

[30] Xie, Y., Rao, Y. and Zhang, P., 2022. Streamwise evolution of turbulent flow and heat transfer over channel surfaces with V ribs and V-rib-dimple compound turbulators. International Journal of Thermal Sciences, 179, 107672.

[31] Rahman, Md.A. and Dhiman, S.K., 2024. Investigations on thermo-fluid performance of a milti-pass shell-and-tube heat exchanger with a novel trapezoidal deflector-type baffle plate. Thermal Engineering, 71, pp. 878–889.

[32] Gupta, S., Chaube, A. and Verma, P., 2013. Augmented heat transfer in square ducts with transverse and inclined ribs with and without a gap. International Journal of Current Engineering and Technology, 3(2), pp. 688–694.